Title

Inflammasome-mediated antagonism of type I interferon enhances Rickettsia pathogenesis.

Authors

Burke, Thomas P
Engström, Patrik
Chavez, Roberto A
et al.

Peer reviewed

Inflammasome-mediated antagonism of type I interferon enhances *Rickettsia* pathogenesis

Thomas P. Burke[1,*], **Patrik Engström**[1], **Roberto A. Chavez**[1], **Joshua A. Fonbuena**[1,2], **Russell E. Vance**[1,3], **Matthew D. Welch**[1,*]

[1]Department of Molecular and Cell Biology, University of California, Berkeley, CA USA

[2]Present address: Department of Pathology, Microbiology and Immunology, University of Utah, Salt Lake City, UT USA

[3]Howard Hughes Medical Institute, University of California, Berkeley, CA, USA

Summary

The innate immune system fights infection with inflammasomes and interferons. Facultative bacterial pathogens that inhabit the host cytosol avoid inflammasomes[1–6] and are often insensitive to type I interferons (IFN-I), but are restricted by IFN-γ[7–11]. However, it remains unclear how obligate cytosolic bacterial pathogens, including *Rickettsia* species, interact with innate immunity. Here, we report that the human pathogen *Rickettsia parkeri* is sensitive to IFN-I and benefits from inflammasome-mediated host cell death that antagonizes IFN-I. *R. parkeri*-induced cell death requires the cytosolic lipopolysaccharide (LPS) receptor caspase-11 and antagonizes IFN-I production mediated by the DNA sensor cGAS. The restrictive effects of IFN-I require the interferon regulatory factor IRF5, which upregulates genes encoding guanylate binding proteins (GBPs) and inducible nitric oxide synthase (iNOS), which we found to inhibit *R. parkeri*. Mice lacking both IFN-I and IFN-γ receptors succumb to *R. parkeri*, revealing critical and overlapping roles for these cytokines *in vivo*. The interactions of *R. parkeri* with inflammasomes and interferons are similar to those of viruses, which can exploit the inflammasome to avoid IFN-I[12], are restricted by IFN-I via IRF5[13,14], and are controlled by IFN-I and IFN-γ *in vivo*[15–17]. Our results suggest that the innate immune response to an obligate cytosolic pathogen lies at the intersection of anti-bacterial and anti-viral responses.

Interferons and inflammasomes constitute two critical arms of innate immunity. Interferons are signaling molecules that upregulate antimicrobial genes to protect the cytosol. Interferons-α and -β (type I interferons or IFN-I) have a nearly universal anti-viral role[18,19],

whereas many bacterial pathogens are instead highly sensitive to restriction by IFN-γ[10,20]. The IFN-I response is antagonized by inflammasomes[21–23], which detect microbial ligands in the cytosol and protect against infection by causing pyroptosis, a rapid lytic host cell death that exposes intracellular microbes to the extracellular space[24,25]. Inflammasomes cause cell death by activating caspase-1 and/or caspase-11, which then cleave and activate the pore-forming protein gasdermin D (GSDMD)[24–26]. Many facultative cytosolic bacterial pathogens including *Listeria monocytogenes* and *Francisella novicida* benefit from IFN-I signaling in vivo[8,27], and avoid inflammasomes by modifying, downregulating, or minimizing ligands recognized by inflammasomes, including lipopolysaccharide (LPS)[4,6], flagellin[17,18], and DNA[4,18,19]. However, it remains unknown whether or how interferons and inflammasomes protect against bacterial pathogens that obligately inhabit the cytosol, such as *Rickettsia* species, which like viruses are absolutely dependent on the cytosolic environment for their replication. Unraveling how interferons and inflammasomes affect obligate cytosolic bacterial pathogens is critical for understanding how the innate immune system discriminates between and targets the variety of pathogens that inhabit the cytosol.

We sought to characterize the role of interferons in restricting the obligate cytosolic human pathogen *Rickettsia parkeri,* which causes eschar-associated rickettsiosis[28]. We observed that IFN-β caused a robust, dose-dependent restriction of *R. parkeri* growth in mouse bone marrow-derived macrophages (BMDMs, Fig. 1a), but did not affect the abundance of *L. monocytogenes* (Extended Data Fig. 1a). Infection with *R. parkeri* also did not induce appreciable IFN-I secretion, unlike infection with *L. monocytogenes* (Extended Data Fig. 1b). We hypothesized that, similar to some DNA viruses[12], *R. parkeri* tolerates inflammasome activation and host cell death to curtail the IFN-I response. We tested for inflammasome activation and observed that *R. parkeri* infection induced ~40% death of wild type (WT) BMDMs at 24 hours post infection (h.p.i.; Fig. 1B). Host cell death was reduced upon infection of cells mutated for *Casp11,* the gene encoding the receptor for cytosolic lipopolysaccharide (LPS)[29], and in *Gsdmd*$^{-/-}$ BMDMs, and was abolished in *Casp1*$^{-/-}$*Casp11*$^{-/-}$ (*Casp1/11*$^{-/-}$) double mutant cells (Fig. 1b), confirming inflammasome activation and pyroptosis by *R. parkeri.* In agreement with our hypothesis, bacteria were moderately restricted in *Casp11*$^{-/-}$ or *Gsdmd*$^{-/-}$ cells, severely restricted in *Casp1/11*$^{-/-}$ cells (Fig. 1c), and bacterial restriction correlated with increased secretion of IFN-I (Fig. 1d). IFN-I production by infected *Casp1/11*$^{-/-}$ cells occurred with similar timing as cell death of infected WT BMDMs (Extended Data Fig. 1c,d), suggesting that cell death antagonizes IFN-I. Furthermore, secreted IFN-I was responsible for *R. parkeri* restriction, as transfer of conditioned supernatant from infected *Casp1/11*$^{-/-}$ cells to infected WT BMDMs caused a dose-dependent inhibition of bacterial growth, whereas supernatant transfer to infected interferon-α/β receptor mutant (*Ifnar*$^{-/-}$) BMDMs had no effect on bacterial growth (Fig. 1e). Moreover, treatment of *Casp1/11*$^{-/-}$ cells with an anti-IFNAR antibody restored *R. parkeri* growth, and BMDMs from triple mutant *Casp1*$^{-/-}$*Casp11*$^{-/-}$*Ifnar*$^{-/-}$ mice supported *R. parkeri* growth (Fig. 1f). Similar experiments showed no role for TNF-α, IL-18, or IL-1β in restricting *R. parkeri* in WT or *Casp1/11*$^{-/-}$ BMDMs (Extended Data Fig. 1f,g). Together, these findings demonstrate that *R. parkeri* is sensitive to IFN-I-mediated killing but avoids stimulating a robust IFN-I response by exploiting the inherent trade-off between inflammasome activation and IFN-I production.

We next sought to determine the mechanism by which *R. parkeri* induces IFN-I production in *Casp1/11*$^{-/-}$ cells by distinguishing whether the host DNA-sensing pathway (cGAS/STING) or LPS-sensing pathway (TLR4) were required for IFN-I production. We infected BMDMs from triple mutant mice and observed that *Casp1*$^{-/-}$*Casp11*$^{-/-}$*Tlr4*$^{-/-}$ cells produced increased IFN-I comparable to *Casp1/11*$^{-/-}$ cells. In contrast, IFN-I secretion from *Casp1*$^{-/-}$*Casp11*$^{-/-}$*Cgas*$^{-/-}$ or *Casp1*$^{-/-}$*Casp11*$^{-/-}$*Sting*$^{-/-}$ BMDMs was comparable to levels from WT cells (Fig. 1g, Extended Data Fig. 1h), and *R. parkeri* growth was supported in these cells (Fig. 1h). These data demonstrate that IFN-I production, which is masked by the inflammasome during *R. parkeri* infection of WT macrophages, depends on cGAS. We propose that lysed *R. parkeri* releases cytosolic DNA that activates cGAS, as well as LPS that activates caspase-11, and that the more rapid pyroptosis curtails the slower transcriptional-based IFN-I response. These findings suggest that a subpopulation of *R. parkeri* is killed in the cytosol, eliciting host cell death that protects the remaining population from an anti-rickettsial IFN-I response.

It remained unclear how *R. parkeri* is restricted by IFN-I. To investigate this, we first sought to identify an interferon-responsive transcription factor (IRF) required for controlling infection. We compared bacterial growth in WT versus *Irf1*$^{-/-}$, *Irf3*$^{-/-}$*Irf7*$^{-/-}$, or *Irf5*$^{-/-}$ mutant BMDMs, and found that growth was increased by mutation of *Irf5* (Fig. 2a). This suggested that IRF5 is primarily responsible for regulating expression of interferon-stimulated genes (ISGs) with anti-rickettsial activity. To identify the ISGs regulated by IRF5, we performed high-throughput RNA-sequencing (RNAseq) at 12 hpi, the earliest time when bacterial killing was observed (Extended Data Fig. 2a). We found that 136 genes were upregulated >4.0-fold in infected WT IFN-I-treated cells when compared to infected untreated cells (Supplementary Dataset). Of these, 36 genes had lower expression in *Irf5*$^{-/-}$ cells compared with *Irf1*$^{-/-}$ and *Irf3*$^{-/-}$*Irf7*$^{-/-}$ cells, indicating that these were substantially and specifically upregulated by IRF5 (Fig. 2b, Extended Data Fig. 2b). Many of the 36 genes encode known anti-microbial proteins, including GBP2, GBP5, VIPERIN (encoded by *Rsad2*), IFIT1, and IFIT2. Expression of *Nos2,* which encodes the known anti-rickettsial factor iNOS[30–33], was also highly dependent on IRF5, although it was also dependent on IRF1. To determine if any of these factors restrict *R. parkeri,* we infected WT and mutant BMDMs carrying mutations in candidate anti-rickettsial genes in the presence of IFN-I. Only BMDMs lacking the chromosome 3 cluster of *Gbp* genes (*Gbp*^{chr3})[34] supported increased bacterial growth compared with WT BMDMs when treated with IFN-I (Fig. 2c, Extended Data Fig. 2c) or IFN-γ (Fig. 2d). Upon iNOS inhibition, bacterial growth was further increased in WT and *Gbp*$^{chr3-/-}$ cells (Fig. 2e, Extended Data Fig. 2d). Together, these results suggest that inflammasome activation allows *R. parkeri* to avoid IFN-I production and downstream expression of anti-rickettsial ISGs, including those encoding GBPs and iNOS.

We hypothesized that these anti-microbial factors were also involved with killing *R. parkeri* upon initial entry to the cytosol, prior to IFN-I induction. We measured host cell death in WT and mutant BMDMs lacking the ISGs identified above and observed that cell death was significantly reduced in *Gbp*$^{chr3-/-}$ cells (Fig. 2f). Despite reduced host cell death, *Gbp*$^{chr3-/-}$ cells did not exhibit increased IFN-I production (Fig. 2g), leading us to conclude that the GBPs are required for bacteriolysis to stimulate cGAS and caspase-11. Consistent

with a role for GBPs in bacterial restriction, GBP2 localized to the surface of ~1–2% *R. parkeri* in untreated WT cells, and the percentage of bacteria with surface-associated GBP2 increased in *Casp1/11⁻/⁻* cells after 12 hpi, correlating with the increase in IFN-I (Fig. 2h,i, Extended Data Fig. 2e). Moreover, co-localization increased upon exogenous IFN-β treatment, and no surface-associated GBP2 was observed in *Gbp^chr3−/−* BMDMs (Extended Data Fig. 2f). These observations suggest that GBP2 directly targets *R. parkeri*, and that the GBPs also have an indirect protective effect by eliciting host cell death in a subset of infected cells. The requirement for GBPs to elicit host cell death early during infection suggests that they act constitutively, and their increased colocalization upon IFN-I treatment further suggests an inducible protective role.

We next evaluated the role for the inflammasome, IFN-I, and IFN-γ in controlling *R. parkeri in vivo*. In agreement with our observations *in vitro*, we observed significantly more IFN-I in spleens of infected *Casp1/11⁻/⁻* versus WT mice, and IFN-I induction depended on cGAS, as it was reduced in *Casp1⁻/⁻Casp11⁻/⁻Cgas⁻/⁻* mice (Fig. 3a; mice separated based on sex in Supplementary Fig. 1). Elevated IFN-I had a direct anti-rickettsial effect in the spleen, as *Casp1⁻/⁻Casp11⁻/⁻Ifnar⁻/⁻* and *Casp1⁻/⁻Casp11⁻/⁻Cgas⁻/⁻* mice had higher bacterial burdens than *Casp1/11⁻/⁻* mice (Fig 3b). Neutralization of IFN-γ caused a modest increase in bacterial burdens in WT and *Casp1/11⁻/⁻* mice and caused a dramatic increase in *Casp1⁻/⁻Casp11⁻/⁻Ifnar⁻/⁻* mice (Fig. 3b, Extended Data Fig. 3a), suggesting that protection by these cytokines is overlapping. It remains unclear why spleens of *Casp1/11⁻/⁻* mice, which express more IFN-β transcript, do not exhibit reduced bacterial burdens when compared to those of WT mice, as we observed for BMDMs *in vitro*. Nevertheless, our observations suggest that bacterial activation of the inflammasome limits the production of cGAS-induced IFN-I, and that IFN-I and IFN-γ are anti-rickettsial in the spleen. We conclude that the relationship between the inflammasome, IFN-I, and IFN-γ in spleens during infection *in vivo* is similar to infection of BMDMs *in vitro*.

In contrast with the results from the spleen, we observed that *Casp1/11⁻/⁻* mice had increased bacterial burdens in the liver. This was dependent on IFN-I because bacterial burdens were reduced to WT levels in *Casp1⁻/⁻Casp11⁻/⁻Ifnar⁻/⁻* and *Casp1⁻/⁻Casp11⁻/⁻Cgas⁻/⁻* animals (Fig. 3c). We hypothesized that the increased bacterial burdens in *Casp1/11⁻/⁻* mice was due to IFN-I-mediated antagonism of IFN-γ, as was previously observed in the liver during *L. monocytogenes* infection[11]. In support of this hypothesis, neutralization of IFN-γ erased the differences observed between *Casp1/11⁻/⁻* and *Casp1⁻/⁻Casp11⁻/⁻Ifnar⁻/⁻* mice (Fig. 3c). Together, these data agree with previous findings that the inflammasome has differing roles in spleens and livers[35], and that IFN-I antagonizes IFN-γ in the liver[11] (schematic in Fig. 3d). The mechanism for IFN-I-mediated antagonism of IFN-γ during infection in the liver remains unclear, and further investigations are required to better understand the cell types that harbor *R. parkeri* and the cells that mediate interferon signaling during infection.

IFN-I acts together with IFN-γ to provide overlapping protection against viral infection in vivo[15,16], whereas IFN-γ dominates the protective response to facultative cytosolic bacterial pathogens[8,11,27]. We therefore tested the roles for IFN-I and IFN-γ in protecting against *R. parkeri* at the whole animal level by intravenously (i.v.) infecting C57BL/6 mice deficient

for both IFN-I and IFN-γ receptors (*Ifnar*$^{-/-}$*Ifngr*$^{-/-}$). Strikingly, infection of *Ifngr*$^{-/-}$*Ifnar*$^{-/-}$ mice caused a loss of body weight and temperature (Extended Data Fig. 3b,c) as well as dose-dependent lethality (Fig. 4a). We observed similar susceptibility in AG129 mice, a different genetic background carrying mutations in *Ifnar* and *Ifngr* (Extended Data Fig. 3d). In contrast, WT, *Ifnar*$^{-/-}$, and *Ifngr*$^{-/-}$ mice had no signs of severe disease even at the highest infectious dose. *Ifngr*$^{-/-}$*Ifnar*$^{-/-}$ mice retained high burdens of *R. parkeri* in spleens and livers (Fig. 4b), which was similar to the abundance that we observed in *Casp1*$^{-/-}$*Casp11*$^{-/-}$*Ifnar*$^{-/-}$ mice treated with the anti-IFN-γ antibody (Fig. 3b,c), suggesting that the most critical consequences of inflammasome activation on *R. parkeri* are the effects that the inflammasome has on both IFN-I and IFN-γ. Livers and spleens were also analyzed for evidence of pathology, and consistent with the increased susceptibility and bacterial burdens, tissues from infected *Ifnar*$^{-/-}$*Ifngr*$^{-/-}$ mice showed marked inflammation, vascular damage, and leukocyte infiltration (Extended Data Fig. 4), similar to clinical features of human *R. parkeri* infections[28]. Our findings that *Ifnar*$^{-/-}$*Ifngr*$^{-/-}$ mice sustained tissue damage and succumbed to infection demonstrate that both interferons play critical overlapping roles in protecting against *R. parkeri* infection. In contrast, upon infection with *L. monocytogenes,* we found that *Ifnar*$^{-/-}$ mice were less susceptible than WT, while *Ifngr*$^{-/-}$ and *Ifngr*$^{-/-}$*Ifnar*$^{-/-}$ mice had similar, increased susceptibilities when compared to WT (Fig. 4c). Overall, our findings that IFN-I significantly protects against *R. parkeri* contrasts with the role for IFN-I in protecting against *L. monocytogenes in vivo*, as well as *Francisella novicida*[7], and pathogens which reside in membrane-bound compartments, including *Salmonella spp.*[36]*, Mycobacterium tuberculosis*[37]*, Coxiella burnetii*[38]*, Chlamydia muridarum*[39]*, and Brucella abortus*[40].

There are currently limited *in vivo* tools for identifying and examining *R. parkeri* virulence factors. Our findings that *Ifnar*$^{-/-}$*Ifngr*$^{-/-}$ mice rapidly succumb to infection are of strong practical importance, as they suggest that the *Ifnar*$^{-/-}$*Ifngr*$^{-/-}$ mouse may serve as an animal model to identify and characterize bacterial virulence genes. As a proof of concept, we infected *Ifnar*$^{-/-}$*Ifngr*$^{-/-}$ mice with an *R. parkeri* mutant lacking outer membrane protein B (OmpB)[41]. In contrast with WT bacteria, infection with the *ompB* mutant caused no lethality in *Ifnar*$^{-/-}$*Ifngr*$^{-/-}$ mice (Fig. 4d). This demonstrates the potential for this animal model to reveal *R. parkeri* virulence genes *in vivo*.

Finally, we investigated the role of cell-extrinsic immunity in protecting against *R. parkeri* by infecting mice depleted for natural killer (NK) or CD8$^+$ T cells and also *Rag2*$^{-/-}$ mice, which lack functional B and T cells altogether. We observed no dramatic increase in bacterial burdens in any of these mice, and *Rag2*$^{-/-}$ mice survived infection with no noticeable symptoms of disease (Extended Data Fig. 5). This demonstrates that the interferon-mediated cell-autonomous response is critical, whereas the cell-extrinsic NK, B and T cell-mediated response is dispensable for controlling *R. parkeri*.

Overall, our findings reveal unexpected differences between the host response to an obligate cytosolic bacterial pathogen and facultative cytosolic bacterial pathogens. Upon infection with facultative cytosolic bacterial pathogens, IFN-γ dominates the protective response *in vivo*[11,36,37], activation of IRF1 is protective[42], and IFN-I does not substantially contribute to protection[7–9]. Moreover, facultative cytosolic pathogens have evolved multiple mechanisms

to avoid inflammasomes[1–6] and some cause increased lethality in inflammasome-deficient mice[43,44]. We instead observe that the host response to *R. parkeri* shares many similarities to the response to viruses. Both *R. parkeri* and viruses are sensitive to IFN-I[17,45] and both benefit from inflammasome-mediated antagonism of IFN-I (Fig. 4e)[12]. We also observe no lethality upon *R. parkeri* infection of inflammasome-deficient mice. Furthermore, the host protects against viral infection with IRF5-regulated genes[13,14] and IFN-I and IFN-γ play overlapping protective roles against viruses[30–32], which we observe for *R. parkeri*. We propose that *R. parkeri* exhibits an intermediate degree of interferon susceptibility between viruses and facultative cytosolic bacterial pathogens (Fig. 4f). *Rickettsia* species have undergone extensive genome reduction[46] and like viruses are absolutely dependent on host processes for replication. We propose that IFN-I alters the cytosol to an uninhabitable environment for obligate microorganisms; this may occur through a combination of ISGs[47] and alterations to metabolism[48]. This study highlights that the principles of innate immunity established by studying facultative bacterial pathogens do not necessarily apply to *R. parkeri and* may not apply to other obligate cytosolic pathogens. Further investigations into obligate bacteria will illuminate how hosts protect the cytosol from infection.

Methods

Preparation of *R. parkeri*

R. parkeri strain Portsmouth was originally obtained from Christopher Paddock (Centers for Disease Control and Prevention). Bacteria were amplified by infecting confluent T175 flasks of female African green monkey kidney epithelial Vero cells were obtained from the UC Berkeley Cell Culture Facility, where they were tested for mycoplasma contamination, and were authenticated by mass spectrometry experiments. Vero cells were grown in DMEM (Gibco 11965–092) with glucose (4.5 g/L) supplemented with 2% fetal bovine serum (FBS, GemCell) with 5×10^6 *R. parkeri* per flask. Infected cells were scraped and collected at 5 days post infection (dpi) when ~90% of cells were highly infected. Scraped cells were centrifuged at 12,000 x G for 20 min at 4°C. Pelleted cells were then resuspended in K-36 buffer (0.05 M KH_2PO_4, 0.05 M K_2HPO_4, 100 mM KCl, 15 mM NaCl, pH 7) and dounced (60 strokes) at 4°C. The solution was then centrifuged at 200 x G for 5 min at 4°C to pellet host cell debris. Supernatant containing *R. parkeri* was overlaid on a 30% MD-76R (Merry X-Ray) solution. Gradients were centrifuged at 18,000 rpm in an SW-28 ultracentrifuge swinging bucket rotor (Beckman/Coulter) for 20 min at 4°C to separate host cells debris. Bacterial pellets were resuspended in brain heart infusion (BHI) media (BD, 237500) and stored at −80°C.

Titers were determined via plaque assays by serially diluting the bacteria in 6-well plates containing confluent Vero cells. Plates were then spun for 5 min at 300 x G in an Eppendorf 5810R centrifuge. At 24 hpi, the media from each well was aspirated and the wells were overlaid with 4 ml/well DMEM with 5% FBS and 0.7% agarose (Invitrogen, 16500–500). At 6 dpi, an overlay of 0.7% agarose in DMEM containing 2.5% neutral red (Sigma, N6264) was added and plaques were counted 24 h later. For infections with *ompB* mutant bacteria, the *ompB^STOP*::TN mutant was used, which contains a transposon and an upstream stop codon in *ompB*[41].

Deriving bone marrow macrophages

To obtain bone marrow, male or female mice were euthanized, and femurs, tibias, and fibulas were excised. Connective tissue was removed, and the bones were sterilized with 70% ethanol. Bones were washed with BMDM media (20% HyClone FBS, 1% sodium pyruvate, 0.1% β-mercaptoethanol, 10% conditioned supernatant from 3T3 fibroblasts, in Gibco DMEM containing glucose and 100 U/ml penicillin and 100 μg/ml streptomycin) and ground using a mortar and pestle. Bone homogenate was passed through a 70 μm nylon Corning Falcon cell strainer (Thermo Fisher Scientific, 08–771-2) to remove particulates. Filtrates were centrifuged in an Eppendorf 5810R at 1,200 RPM (290 x G) for 8 min, supernatant was aspirated, and the remaining pellet was resuspended in BMDM media. Cells were then plated in non-TC-treated 15 cm petri dishes (at a ratio of 10 dishes per 2 femurs/tibias) in 30 ml BMDM media and incubated at 37° C. An additional 30 ml was added 3 d later. At 7 d the media was aspirated, and cells were incubated at 4°C with 15 ml cold PBS (Gibco, 10010–023) for 10 min. BMDMs were then scraped from the plate, collected in a 50 ml conical tube, and centrifuged at 1,200 RPM (290 x G) for 5 min. The PBS was then aspirated, and cells were resuspended in BMDM media with 30% FBS and 10% DMSO at 10^7 cells/ml. 1 ml aliquots were stored in liquid nitrogen.

Infections *in vitro*

To plate cells for infection, aliquots of BMDMs were thawed on ice, diluted into 9 ml of DMEM, centrifuged in an Eppendorf 5810R at 1,200 RPM (290 x G) for 5 minutes, and the pellet was resuspended in 10 ml BMDM media without antibiotics. The number of cells was counted using Trypan blue (Sigma, T8154) and a hemocytometer (Bright-Line), and 5×10^5 cells were plated into 24-well plates. Approximately 16 h later, 30% prep *R. parkeri* were thawed on ice and diluted into fresh BMDM media to the desired concentration (either 10^6 PFU/ml or 2×10^5 PFU/ml). Media was then aspirated from the BMDMs, replaced with 500 μl media containing *R. parkeri,* and plates were spun at 300 G for 5 min in an Eppendorf 5810R. Infected cells were then incubated in a humidified CEDCO 1600 incubator set to 33°C and 5% CO_2 for the duration of the experiment. For treatments with recombinant mouse IFN-β, IFN-β (PBL, 12405–1) was added directly to infected cells immediately after spinfection. To obtain conditioned supernatant from infected *Casp1/11$^{-/-}$* cells, BMDMs were infected at an MOI of 1 in a volume of 500 μl fresh media. At 24 hpi, conditioned media was pooled from 30 wells and frozen at −80° C. For treatment of infected cells with this conditioned supernatant, the indicated volumes of media were removed at 20 minutes post spinfection and replaced with an equal amount of the thawed conditioned media. To neutralize IFN-I signaling, an ultra-LEAF-purified α-IFNAR-1 antibody (BioLegend, 127323) was added to a final concentration of 1 μg/ml at 0 hpi. IFN-γ (R&D Systems, 485-MI-100) was added to the wells immediately after spinfection. IL-1β was neutralized by adding the ULTRA-Leaf α-IL-1β antibody (BioLegend 503514) to a final concentration 1 μg/ml at t=0. IL-18 was neutralized by adding the α-IL-18 antibody (MBL, D048–3) to 5 μg/ml at t=0. Control IgG antibody (5 μg, Jackson, 012–000-003) was added at t=0. For experiments with recombinant TNF-α, 200 ng was added to each well in a 24-well plate, and two different products were tested (BioLegend 575202; Thermo Fisher Scientific PMC3014).

For measuring PFU, supernatants from infected BMDMs were aspirated from individual wells, and each well was gently washed twice with 500 μl sterile milli-Q-grade water. 1 ml of sterile milli-Q water was then added to each well and repeatedly pipetted up and down to lyse the host cells. Serial dilutions of lysates were added to confluent Vero cells in 12 well plates that were plated 24 or 48 h prior. Plates were then spun at 300 x G using an Eppendorf 5810R centrifuge for 5 min at room temperature and incubated at 33°C overnight. At ~16 hpi, media was aspirated and replaced with 2 ml/well of DMEM containing 0.7% agarose and 5% FBS. At ~6 dpi, 1 ml of DMEM containing 0.7% agarose, 1% FBS, 200 μg/ml amphotericin B (Invitrogen, 15290–018), and 2.5% neutral red (Sigma) was added to each well. Plaques were counted 24 h later.

For collecting supernatant from $Casp1/11^{-/-}$ cells, 5×10^5 BMDMs in 24-well plates were infected with *R. parkeri* at an MOI of 1 and at 24 hpi supernatants were pooled and stored at −80°C. For adding the supernatant to infected BMDMs, either 200 or 500 μl of supernatant was removed at 20 min post infection (mpi) from the untreated cells and replaced with the supernatant from $Casp1/11^{-/-}$ cells.

For infections with *L. monocytogenes,* cultures of *L. monocytogenes* strain 10403S (originally obtained from Dr. Dan Portnoy, UC Berkeley) were grown in 2 ml sterile-filtered BHI shaking at 37°C to stationary phase (~16 h). Cultures were centrifuged at 20,000 x G (Eppendorf 5430), the pellet was resuspended in sterile PBS and diluted 100-fold in PBS. 10 μl of the diluted bacteria were then added to each well of a 24-well plate of BMDMs that were plated ~16 h prior to infections at 5×10^5 cells/well. Bacteria were also plated out onto Luria Broth agarose plates to determine the titer, which was determined to be ~5×10^5 bacteria / 10 μl, for an MOI of 1 (based on the ratio of bacteria in culture to number of BMDMs). Infected cells were incubated in a humidified 37° incubator with 5% CO_2. 25 μg of gentamicin (Gibco 15710–064) was added to each well (final concentration 50 μg/ml) at 1 hpi. At 30 mpi, 2, 5, and 8 hpi, the supernatant was aspirated from infected cells, and cells were washed twice with sterile milli-Q water. Infected BMDMs were then lysed with 1 ml sterile water by repeated pipetting and scraping of the well. Lysates were then serially diluted and plated on LB agar plates, incubated at 37° overnight, and colony forming units were counted at ~20 h later.

High-throughput RNA sequencing

For high-throughput RNA sequencing, 5×10^5 BMDMs were plated in 24-well plates and infected 16 h later with *R. parkeri* and treated with 10,000 activity units of recombinant IFN-β. To determine the percentage of cells that were successfully infected, we analyzed the infected cells using immunofluorescence microscopy and observed that the multiplicity of infection (the average number of bacteria per host cell) was 2.3, and that 71% of cells were infected. At 12 hpi, cells were lysed and RNA was purified using an RNeasy purification kit (Qiagen). RNA quality was assessed using an Agilent 2100 Bioanalyzer, and all samples had RNA integrity numbers (RIN) values above 8.0. Transcripts were selected using polyA selection (using Dynabeads mRNA Purification Kit, Invitrogen) and enzymatically fragmented as part of the Apollo library prep kits (Wafergen PrepX RNA library prep for Illumina). Libraries were constructed by using Apollo 324 (IntegenX Inc.), PCR-amplified,

and multiplexed at the Functional Genomics Lab at the University of California, Berkeley (https://genomics.qb3.berkeley.edu). The resulting libraries were sequenced at the Vincent J. Coates Genomics Sequencing Facility at the University of California, Berkeley using single-end reads, 50 base length, with the Hiseq 2000 Illumina platform. Sequence data were aligned to the *Mus musculus* C57BL/6 reference genome (reference assembly GCA_000001635.8) using CLC Genomics Workbench (Qiagen). Fold regulation for each genotype was determined by a ratio to the uninfected, untreated BMDMs. Comparisons were then made between the sequencing results from the infected, IFN-I-treated WT and the *Irf* mutant genes. Each data set was composed of at least 55 million reads and 98.3% of the reads aligned with the reference. Genes with low abundance of reads (Reads Per Kilobase of transcript, per Million mapped reads, RPKM, of <10) in the infected WT BMDMs treated with IFN-I were excluded from the analysis.

Microscopy

For immunofluorescence microscopy, 2.5×10^5 BMDMs were plated overnight in BMDM media in 24-well plates with sterile 12 mm coverslips (Thermo Fisher Scientific, 12–545-80). Infections were performed as described above. At the indicated times post-infection, coverslips were washed once with PBS and fixed in 4% paraformaldehyde (Ted Pella Inc., 18505, diluted in 1 x PBS) for 10 min at room temperature. Coverslips were then washed 3 times in PBS. Coverslips were washed once in blocking buffer (1 x PBS with 2% BSA) and permeabilized with 0.5% triton X-100 for 10 min. Coverslips were incubated with antibodies diluted in 2% BSA in PBS for 30 min at room temperature. *R. parkeri* was detected using mouse anti-*Rickettsia* 14–13 (originally from Dr. Ted Hackstadt, NIH/NIAID Rocky Mountain Laboratories). GBP2 was detected with anti-GBP2 (ProteinTech, rabbit polyclonal, 11854–1-AP; Research Resource Identifier AB_2109336). Nuclei were stained with DAPI, and actin was stained with Alexa-568 phalloidin (Life Technologies, A12380). Secondary antibodies were Alexa-405 goat anti-mouse (A31553) and Alexa-488 goat anti-rabbit (A11008). Coverslips were mounted in Prolong mounting media (Invitrogen). Samples were imaged with the Nikon Ti Eclipse microscope with a Yokogawa CSU-XI spinning disc confocal with 60X and 100X (1.4 NA) Plan Apo objectives, and a Clara Interline CCD Camera (Andor Technology) using MetaMorph software v.7.8.2.0 (Molecular Devices). Rendered Z-stacks were used for quantifications. Images were processed using FIJI[49] and brightness and contrast adjustments were applied to entire images. Images were assembled using Adobe Illustrator. Representative images are a single optical section, in which most or all bacteria were in the focal plane. For brightfield microscopy, images were captured using an IX71 Olympus microscope with a UCPLFLN 20× 0.7 NA objective, OptiMOS sCMOS camera (QImaging), and Micro-Manager software v.1.4.20[50].

In vitro assays

For LDH assays, 60 μl of supernatant from wells containing BMDMs was collected into 96-well plates. 60 μl of LDH buffer was then added. LDH buffer contained: 3 μ of "INT" solution containing 2 mg/ml tetrazolium salt (Sigma I8377) in PBS; 3 μl of "DIA" solution containing 13.5 units/ml diaphorase (Sigma, D5540), 3 mg/ml β-nicotinaminde adenine dinucleotide hydrate (Sigma, N3014), 0.03% BSA, and 1.2% sucrose; 34 μl PBS with 0.5% BSA; and 20 μl solution containing 36 mg/ml lithium lactate in 10 mM Tris HCl pH 8.5

(Sigma L2250). Supernatant from uninfected cells and from cells completely lysed with 1% triton X-100 (final concentration) were used as controls. Reactions were incubated at room temperature for 20 min prior to reading at 490 nm using an Infinite F200 Pro plate reader (Tecan). Values for uninfected cells were subtracted from the experimental values, divided by the difference of triton-lysed and uninfected cells, and multiplied by 100 to obtain percent lysis. Each experiment was performed and averaged between technical duplicates and biological triplicates.

For the IFN-I bioassay, 5×10^4 3T3 cells containing an interferon-sensitive response element (ISRE) fused to luciferase[51] were plated per well into 96-well white-bottom plates (Greiner 655083) in DMEM containing 10% FBS, 100 U/ml penicillin and 100 μg/ml streptomycin. Media was replaced 24 h later and confluent cells were treated with 2 μl of supernatant harvested from BMDM experiments. Media was removed 4 h later and cells were lysed with 40 μl TNT lysis buffer (20 mM Tris, pH 8, 200 mM NaCl, 1% triton X-100). Lysates were then injected with 40 μl firefly luciferin substrate (Biosynth) and luminescence was measured using a SpectraMax L plate reader (Molecular Devices).

qPCR

For qPCR experiments using mouse tissue, RNA was extracted from 50 μl of organ homogenate collected at 72 hpi using an RNeasy kit (Qiagen). RNA abundance was quantified using a NanoDrop ND-1000 and 200 ng RNA was *in vitro* transcribed (ProtoScript II, NEB, M0368S) and diluted 10x in sterile nuclease-free water. Real-time PCR was performed using SYBR Green (Thermo Fisher Scientific, A25742), 2 μl of cDNA, and 1 μM each of the following oligonucleotides: actin F: GGCTGTATTCCCCTCCATCG; actin R: GTCACCCACATAGGAGTCCTTC; IFN-β F: AGCTCCAAGAAAGGACGAACAT; and IFN-β R: CCCTGTAGGTGAGGTTGATCTT. For normalization, values for IFN-β were divided by values for actin. Measurements were acquired with a QuantStudio 5 real-time qPCR machine (Applied Biosystems).

Animal experiments

Animal research using mice was conducted under a protocol approved by the UC Berkeley Institutional Animal Care and Use Committee (IACUC) in compliance with the Animal Welfare Act and other federal statutes relating to animals and experiments using animals (Welch lab animal use protocol AUP-2016–02-8426). The UC Berkeley IACUC is fully accredited by the Association for the Assessment and Accreditation of Laboratory Animal Care International and adheres to the principles of the Guide for the Care and use of Laboratory Animals. Infections were performed in a biosafety level 2 facility. All animals were maintained at the UC Berkeley campus and all infections were performed in accordance with the approved protocols. Mice were age matched between 8 and 18 weeks old. Mice were selected for experiments based on their availability, regardless of sex. PFU data for each sex is reported in Supplemental Fig. 1. A statistical analysis was not performed to predetermine sample size prior to initial experiments. Initial sample sizes were based on availability of mice and the capacity to process samples within a given time, which was approximately 4 mice per group and 3–4 total groups. After the first experiment, a Power Analysis was conducted to determine subsequent group sizes. All mice were of the

C57BL/6J background except for AG129 mice, which are of the 129 background. All mice were healthy at the time of infection and were housed in microisolator cages and provided chow and water. No mice were administered antibiotics or maintained on water with antibiotics. Experimental groups were littermates of the same sex that were randomly assigned to experimental groups. For experiments with mice mutated for *Ifnar* and *Ifngr*, mice were immediately euthanized if they exhibited severe degree of infection, as defined by a core body temperature dropping below 90° F or lethargy that prevented normal movement around the cage.

Mouse genotyping

Casp1[−/−,52], *Sting*[gt/gt,53], *Cgas*[−/−,54], *Gsdmd*[−/−,52], *Irf5*[−/−,55], *Ifit1*[−/−,56], and *Ifit2*[−/−,57], *LipG*[−/−,58], *Gbp*[chr3−/−,34] mice were previously described. *Casp11*[−/−,59], *Irf1*[−/−,60], *Ifnar*[−/−,17], *Ifngr*[−/−,61], *Ifnar*^{−/−}*Ifngr*^{−/−}, *Rag2*^{−/−} and C57BL/6J WT mice were previously described and originally obtained from Jackson Laboratories. For genotyping, ear clips were boiled for 15 min in 60 µl of 25 mM NaOH, quenched with 10 µl tris-HCl pH 5.5, and 2 µl of lysate was used for PCR using SapphireAMP (Takara, RR350) and primers specific for each gene. Mice were genotyped using these primers: *Ifnar* forward (F): CAACATACTACAACGACCAAGTGTG; *Ifnar* WT reverse (R): AACAAACCCCCAAACCCCAG; *Ifnar*^{−/−} R: ATCTGGACGAAGAGCATCAGG; WT *Casp1/11* F: CATGCCTGAATAATGATCACC; WT *Casp1/11* R: GAAGAGATGTTACAGAAGCC; *Casp1/11*[−/−] F: GCGCCTCCCCTACCCGG; *Casp1/11*[−/−] R: CTGTGGTGACTAACCGATAA; *Cgas* F: ACTGGGAATCCAGCTTTTCACT; *Cgas* R: TGGGGTCAGAGGAAATCAGC; WT *Tlr4* F: CACCTGATACTTAATGCTGGCTGTAAAAAG; WT *Tlr4* R: GGTTTAGGCCCCAGAGTTTTGTTCTTCTCA; *Tlr4*^{−/−} F: TGTTGCCCTTCAGTCACAGAGACTCTG; *Tlr4*^{−/−} R: TGTTGGGTCGTTTGTTCGGATCCGTCG; *Sting* F: GATCCGAATGTTCAATCAGC; *Sting* R: CGATTCTTGATGCCAGCAC; *Gsdmd* F: ATAGAACCCGTGGGAGTCCCA; and *Gsdmd* R: GGCTTCCCTCATTCAGTGCT.

Mouse infections

For mouse infections, *R. parkeri* was prepared by diluting 30%-prep bacteria into 1 ml cold sterile PBS, centrifuging the bacteria at 12,000 x G for 1 min (Eppendorf 5430 centrifuge), and resuspended in cold sterile PBS to the desired concentration (either 5×10^7 PFU/ml, 2.5×10^7 PFU/ml, 5×10^6 PFU/ml, or 5×10^5 PFU/ml). Bacterial suspensions were kept on ice during injections. Mice were exposed to a heat lamp while in their cages for approximately 5 minutes and then each mouse was moved to a mouse restrainer (Braintree, TB-150 STD). The tail was sterilized with 70% ethanol and 200 µl of bacterial suspensions were injected using 30.5-gauge needles into the lateral tail vein. Body temperatures were monitored using a rodent rectal thermometer (BrainTree Scientific, RET-3). For delivering the anti-IFN-γ antibody (BioLegend, 505847), mice were injected i.v. with 300 µl at 30 min p.i., 200 µl at 24 hpi, and 200 µl at 48 hpi, totaling 800 µl (0.8 µg antibody). CD8⁺ T cells were depleted by injecting mice intraperitoneally with 160 µg of α-CD8b.2 (Leinco C2832) on days −2 and −1 prior to infection (320 µg total per mouse). NK cells were depleted by injecting mice intraperitoneally with 200 µg PK136 antibody (a generous gift from Dr. David Raulet) on

days −2 and −1 prior to infection. For control experiments, 100 μg of control IgG antibody (Jackson, 012–000-003) was delivered IP at days −2 and −1. After infection, all mice in this study were monitored daily for clinical signs of disease, such as hunched posture, lethargy, or scruffed fur. Only mice lacking both interferon receptors exhibited such symptoms, and if this occurred, mice were monitored daily for signs of disease, weight, and temperature. If a mouse displayed severe signs of infection, as defined by a reduction in body temperature below 90°F or an inability to move around the cage normally, the animal was immediately and humanely euthanized using CO_2 followed by cervical dislocation, according to IACUC-approved procedures.

For harvesting organs, mice were euthanized at the indicated pre-determined times and doused with ethanol. Mouse organs were extracted and deposited into 50 ml conicals containing 4 ml sterile cold PBS for the spleen and 8 ml for the liver. Organs were kept on ice and were homogenized for ~10 s using an immersion homogenizer (Fisher, Polytron PT 2500E) at 22,000 RPM. Organ homogenates were spun at 290 x G for 5 min to pellet cell debris (Eppendorf 5810R centrifuge). 20 μl of organ homogenates were serial diluted into 12-well plates containing confluent Vero cells. The plates were then spun at 260 x G for 5 min at room temperature (Eppendorf 5810R centrifuge) and incubated at 33°C. To reduce the possibility of contamination, organ homogenates were plated in duplicate and the second replicate was treated with 50 μg/ml carbenicillin (Sigma) and 200 μg/ml amphotericin B (Gibco). The next day, at approximately 16 hpi, the cells were gently washed by replacing the existing media with 1 ml DMEM containing 2% FBS. The media was then aspirated and replaced with 2 ml/well of DMEM containing 0.7% agarose, 5% FBS, and 200 μg/ml amphotericin B. When plaques were visible at 6 dpi, 1 ml of DMEM containing 0.7% agarose, 1% FBS, and 2.5% neutral red (Sigma) was added to each well and plaques were counted 24 h later.

Histology

For histology, spleens and livers were harvested from infected mice at 72 hpi and immediately stored in 10% neutral buffered saline (Sigma HT501128). Histology was performed by HistoWiz Inc. (histowiz.com) using a standard operating procedure and fully automated workflow. Samples were processed, embedded in paraffin, and sectioned at 4 μm thickness. Bond Polymer Refine Detection (Leica Biosystems) was used according to manufacturer's protocol. After staining, sections were dehydrated and film coverslipped using a TissueTek-Prisma and Coverslipper (Sakura). Whole slide scanning (40x) was performed on an Aperio AT2 (Leica Biosystems). Commercial pathology consultation was blindly performed by a pathologist (HistoWiz, Inc).

Statistical analysis

Statistical parameters and significance are reported in the Figure legends. For comparing two sets of data, a two-tailed Student's T test was performed. For comparing multiple data sets, a one-way ANOVA with multiple comparisons with Tukey post-hoc test was used for normal distributions, and a Mann-Whitney *U* test was used for non-normal distributions. Data are determined to be statistically significant when $p<0.05$. All data points shown in bar graphs and in animal data are distinct samples. Asterisks denote statistical significance as: *,

p<0.05; **, p<0.01; ***, p<0.001; ****, p<0.0001, compared to indicated controls. For animal experiments, bars denote medians. Error bars indicate standard deviation (SD). All other graphical representations are described in the Figure legends. Statistical analyses were performed using GraphPad PRISM v.6 and v.7.

Data availability

The RNAseq data sets generated and analyzed during the current study are available in the Gene Expression Omnibus (GEO) repository, accession number GSE128211. *R. parkeri* strains were authenticated by whole genome sequencing and are available in the NCBI Trace and Short-Read Archive; Sequence Read Archive (SRA), accession number SRX4401164.

Extended Data
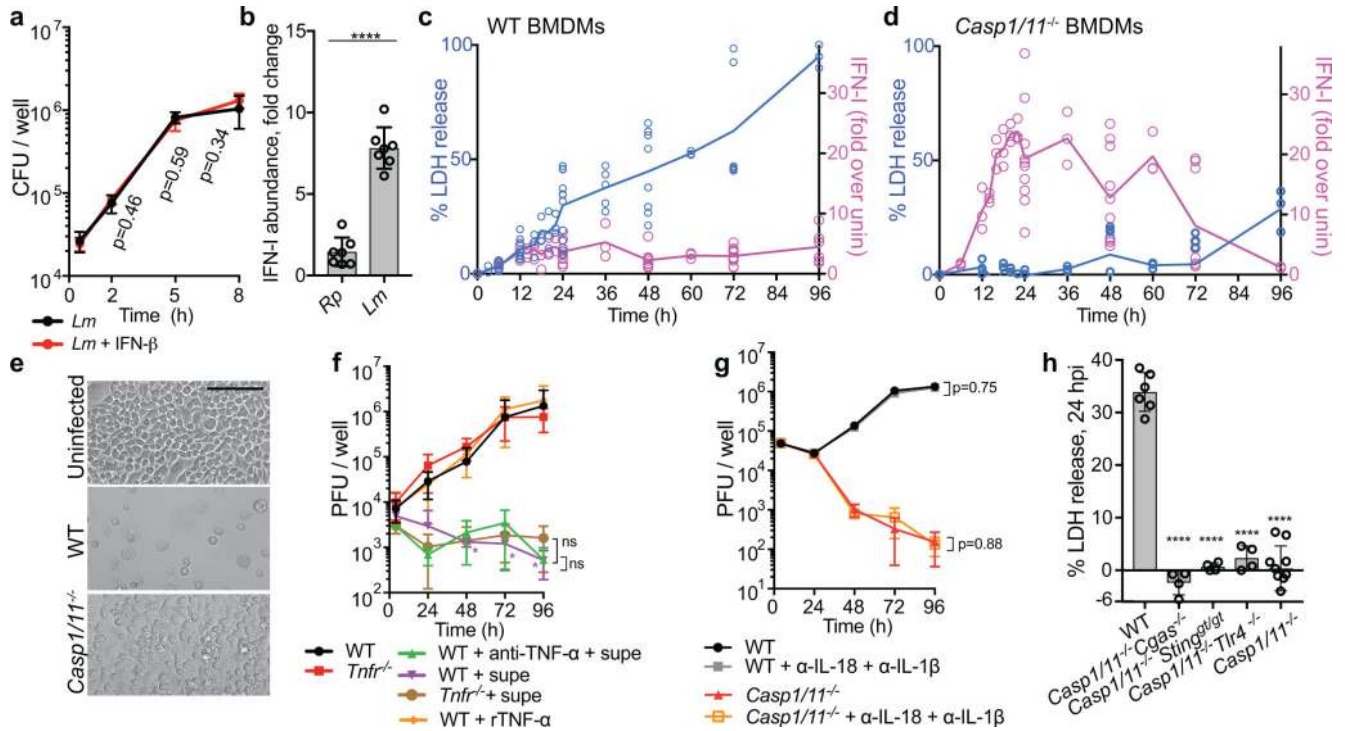
Extended Data Fig. 1. Inflammasome activation benefits *R. parkeri* by antagonizing the IFN-I response in mouse macrophages

a) Measurement of *Listeria monocytogenes* (*Lm*) CFU in BMDMs, MOI of 1. 3,000 U of IFN-β added at t=0. n=3 independent experiments. **b**) Measurement of IFN-I in supernatants of WT BMDMs infected with *R. parkeri* (24 hpi) or *L. monocytogenes* (8 hpi), MOI of 1. Supernatants were used to stimulate a luciferase-expressing cell line and relative light units (RLU) were measured and compared between each sample and uninfected cells. n=7 and 7 biological replicates. **c**) Time course of LDH release (blue) and IFN-I abundance as measured by RLU production (pink), in WT BMDMs infected with *R. parkeri,* MOI of 1. n=3 independent experiments. **d**) Time course of LDH release (blue) and IFN-I abundance (pink), in *Casp1/11^{-/-}* BMDMs infected with *R. parkeri,* MOI of 1. n=3 independent experiments. **e**) Images of BMDMs infected with *R. parkeri*, MOI of 1, at 72 hpi. Scale bar = 100 μm. Experiments were repeated 3 times with similar results. **f**) Measurement of *R. parkeri* abundance in BMDMs, MOI of 0.2. "Supe" indicates 200 μl of conditioned supernatant collected at 24 hpi from *Casp1/11^{-/-}* BMDMs infected at an MOI of 1. Antibody was added at t=0. The indicated statistical differences (*) are between WT and WT + supernatant. No statistical differences were observed between the samples treated with supernatant. **g**) Measurement of *R. parkeri* abundance in BMDMs, MOI of 1. Antibodies were added at t=0. n=3 independent experiments. **h)** Host cell death during *R. parkeri* infection of BMDMs. LDH release was measured at 24 hpi upon *R. parkeri* infection of the indicated BMDMs, MOI of 1. n=6, 4, 4, and 4 biological replicates. Statistical comparisons in panel h were made between each sample and WT. Statistical analyses in panels a, b, f, and g used a two-tailed Student's T-test. Statistical analyses in panel h used a one-way ANOVA with multiple comparisons and Tukey post-hoc test. For all panels: data
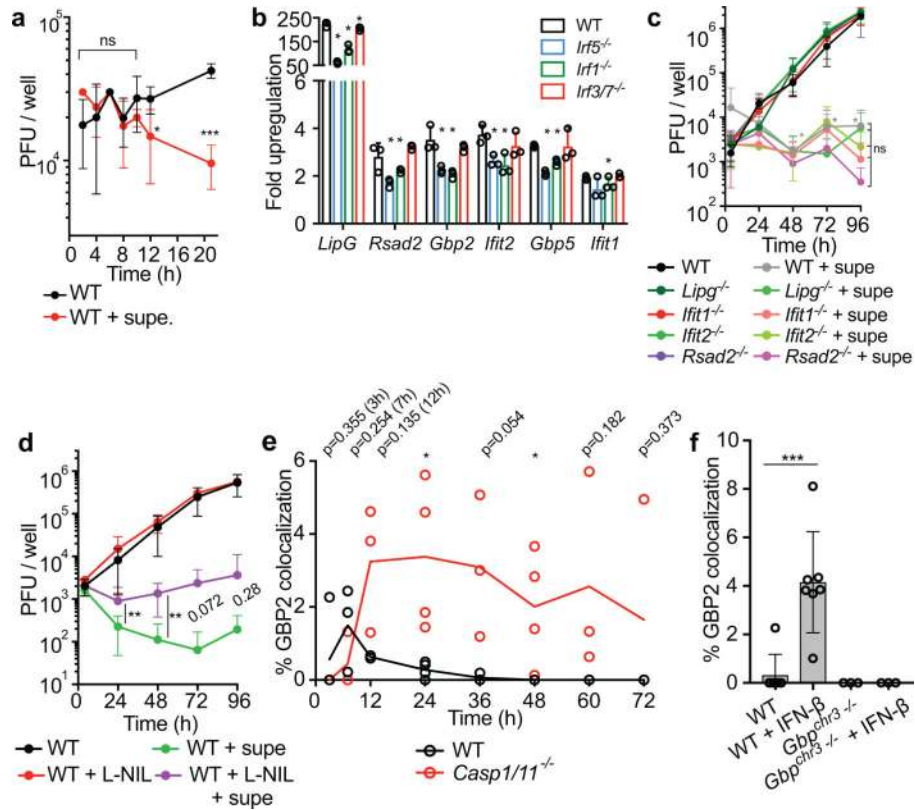
are expressed as means and error bars represent the SD; *p<0.05, **p<0.01, ***p<0.001, ****p<0.0001.

Extended Data Fig. 2. RF5-regulated genes, including *Gbp2* and *Nos2*, are anti-rickettsial ISGs
a) *R. parkeri* abundance in BMDMs. "supe" indicates 200 μl conditioned supernatant from infected *Casp1/11*[−/−] BMDMs. n=3 independent experiments. **b**) qPCR of ISGs, normalized to actin. WT and mutant BMDMs were infected with *R. parkeri* and treated with IFN-β and RNA was analyzed at 12 hpi. Data are fold upregulation as compared to infected cells not treated with IFN-β. n=3 separate experiments. For statistics, values were compared to the WT value for each primer set. **c**) *R. parkeri* abundance in BMDMs. "supe" indicates 200 ul conditioned supernatant from infected *Casp1/11*[−/−] BMDMs. n=3 independent experiments. Statistical differences (*) are shown between WT and WT + supernatant. No statistical differences (ns) were observed between WT + supernatant and mutant cells + supernatant. **d**) *R. parkeri* abundance in BMDMs. "supe" indicates 200 μl conditioned supernatant from infected *Casp1/11*[−/−] BMDMs. The L-NIL final concentration was 1 mM, added at t=0. n=3 independent experiments. **e**) Quantification of GBP2 colocalization with *R. parkeri* using immunofluorescence microscopy, in BMDMs, MOI of 1. Each data point is an independent experiment and includes quantification from more than 5 images totaling at least 150 bacteria. n=3 independent experiments. Lines connect means for each time point. **f**) Quantification of GBP2 colocalization with *R. parkeri* using immunofluorescence microscopy, in BMDMs, MOI of 1 at 3 hpi. Each data point is an independent experiment and includes quantification from more than 5 images totaling at least 150 bacteria. n=7, 7, 3, and 3 independent experiments. For experiments with exogenous IFN-I, 100 U of rIFN-β was added overnight prior to infection. Statistical analyses in panels a, b, c, d, and e used a two-tailed Student's T-test; statistical analyses in panel f used a one-way ANOVA with multiple comparisons and Tukey post-hoc test; For all panels, data are expressed as means
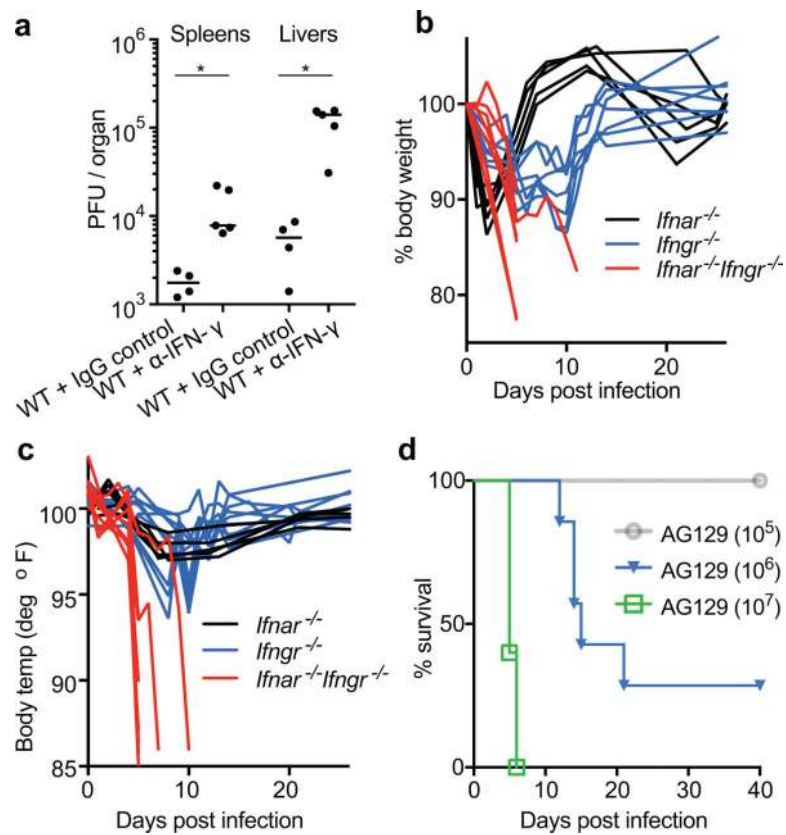
and error bars represent the SD. *$p < 0.05$, **$p < 0.01$, ***$p < 0.001$, ****$p < 0.0001$, ns=not significant.

Extended Data Fig. 3. IFN-I and IFN-γ play overlapping roles in protecting against *R. parkeri in vivo*

a) *R. parkeri* abundance in mouse organs, infected i.v. with 10^7 bacteria, at 72 hpi. Bars denote medians. n=4 (control) and 5 (α-IFN-γ) individual mice, for each organ. Data are the combination of two independent experiments. Each individual data point represents an individual mouse. Statistics used a two-tailed Mann Whitney *U* test. *p<0.05. **b**) Mouse weight after i.v. infection with 10^7 *R. parkeri*. Data are normalized to the weight at t=0. Each line represents an individual mouse. n=5 (*Ifnar*^{−/−}), 7 (*Ifngr*^{−/−}), and 7 (*Ifnar*^{−/−}*Ifngr*^{−/−}). **c**) Mouse body temperature after i.v. infection with 10^7 *R. parkeri*. Each line represents an individual mouse. n=5 (*Ifnar*^{−/−}), 7 (*Ifngr*^{−/−}), and 7 (*Ifnar*^{−/−}*Ifngr*^{−/−}). **d**) Survival of AG129 genotype mice (lacking IFN-I and IFN-γ receptors) after i.v. infection. n=5 (10^7), 7 (10^6), and 5 (10^5). Data for each group are the combination of 2 independent experiments.
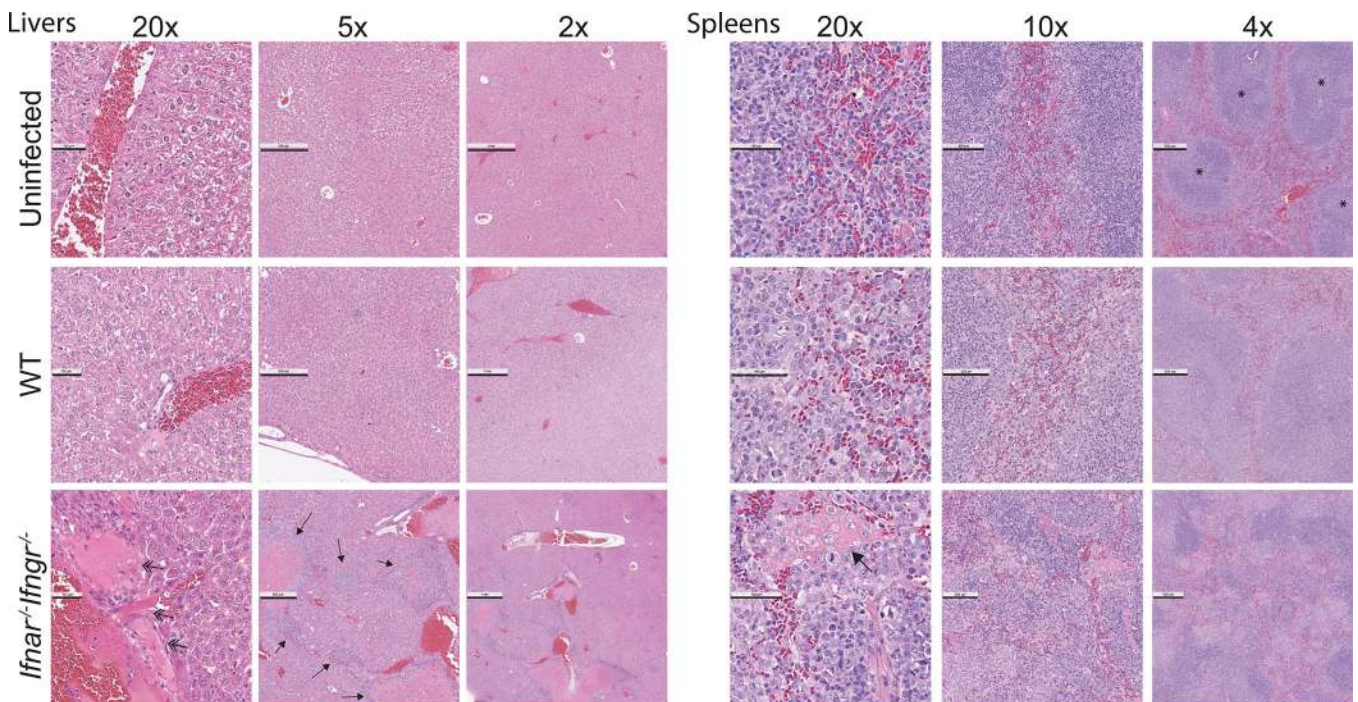
|	Organ	Degree of inflammation and necrosis (0-5)	Degree vascular damage (0-5)
WT uninfected	liver	0	0
WT	liver	2	2
Ifnar⁻/⁻Ifngr⁻/⁻	liver	4	4
WT uninfected	spleen	0	0
WT	spleen	2	1
Ifnar⁻/⁻Ifngr⁻/⁻	spleen	4	3

Grading
0 = none
1 = minimal
2 = mild
3 = moderate
4 = marked
5 = severe

Extended Data Fig. 4. Tissue necrosis, leukocyte infiltration, and vascular damage is increased in spleens and livers of infected *Ifnar*⁻/⁻*Ifngr*⁻/⁻ mice.

Organs were harvested from mice intravenously infected with 10^7 *R. parkeri* at 72 hpi. Samples were fixed, sliced, and stained with hematoxylin and eosin (H&E) and commercially analyzed by a pathologist for inflammation and vascular damage. Inflammation observed was infiltration of mononuclear cells including macrophages, plasma cells, and lymphocytes in both organs, and also granulocytes in the liver. Vascular changes include fibrinoid vascular wall degeneration, hypertrophy of the endothelium, perivascular fibrinous material, and fibrin thrombi in medium caliber vessels. Double-headed arrows indicate aberrations at the vasculature and single-headed arrows indicate regions of necrosis and/or regions of mononuclear infiltrates. Scale bars in the liver are 100 μm (20x), 500 μm (4x) and 1 mm (2x); scale bars in the spleen are 100 μm (20x), 200 μm (10x), and 500 μm (4x); asterisks indicate defined splenic follicles in uninfected mice, which are lost in infected *Ifnar*⁻/⁻*Ifngr*⁻/⁻ mice; results were similar in 3 independent replicates.
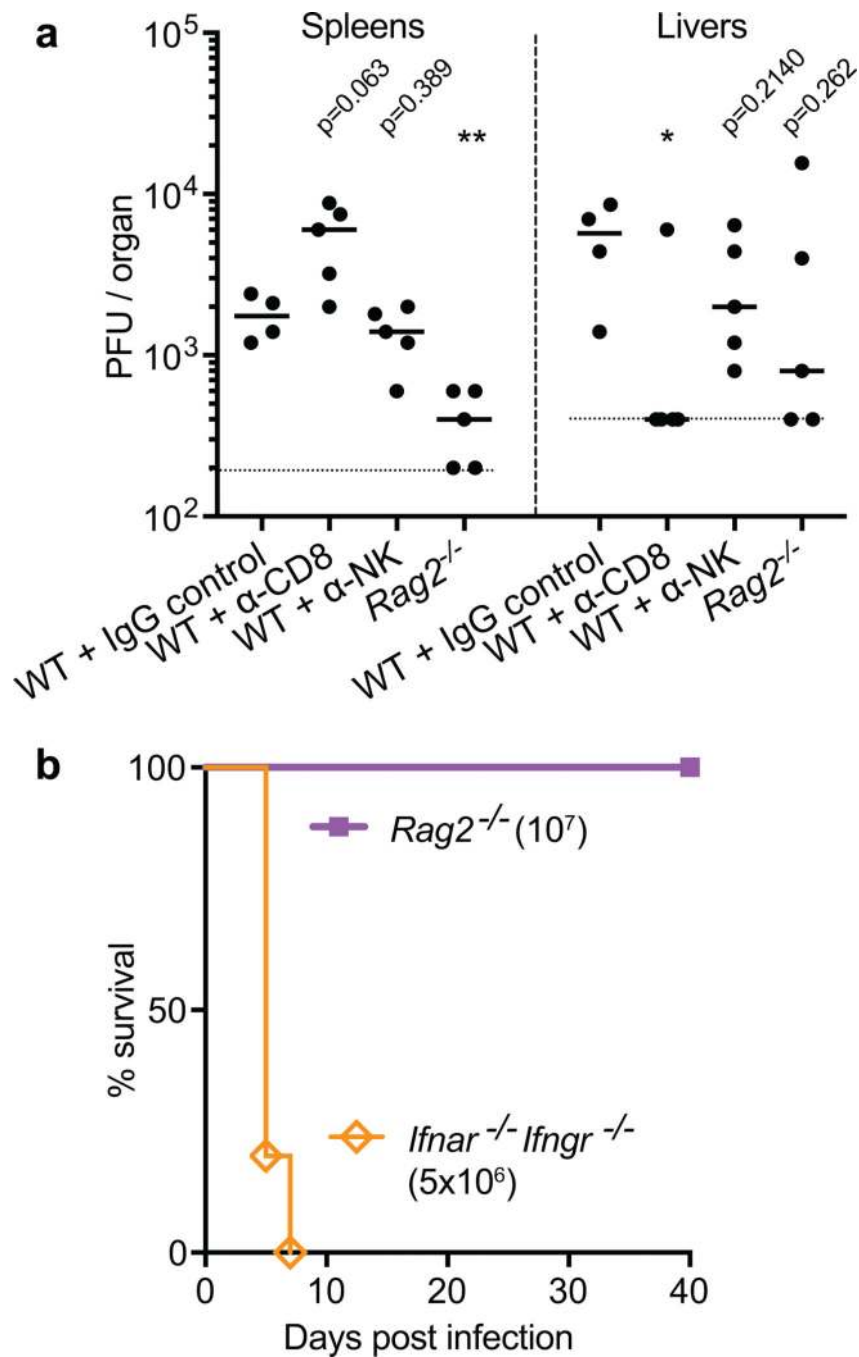
Extended Data Fig. 5. NK and CD8⁺ T cells do not play a critical role in protecting against intravenous *R. parkeri* infection in mice

a) *R. parkeri* abundance in mouse organs, infected i.v. with the indicated amounts of bacteria, at 72 hpi. Bars denote medians. From left to right, n=4, 5, 5, and 5 individual mice, for each organ. Statistics used a two-tailed Mann Whitney *U* test, where each condition was compared to the WT + IgG control for each organ. *p<0.05, **p<0.01, and ns=not significant. **b**) Survival of mice after i.v. infection. n=4 (*Rag2*⁻/⁻) and 5 (*Ifnar*⁻/⁻*Ifngr*⁻/⁻) individual mice. Data for each group are combined from 2 independent experiments.

Supplementary Material

Refer to Web version on PubMed Central for supplementary material.

Acknowledgements

References

1. Shen A & Higgins DE The MogR transcriptional repressor regulates nonhierarchal expression of flagellar motility genes and virulence in Listeria monocytogenes. PLoS Pathog. 2, e30 (2006). [PubMed: 16617375]

2. Sauer J-D et al. Listeria monocytogenes triggers AIM2-mediated pyroptosis upon infrequent bacteriolysis in the macrophage cytosol. Cell Host Microbe 7, 412–419 (2010). [PubMed: 20417169]

3. Sauer J-D et al. Listeria monocytogenes engineered to activate the Nlrc4 inflammasome are severely attenuated and are poor inducers of protective immunity. Proc. Natl. Acad. Sci. U.S.A. 108, 12419–12424 (2011). [PubMed: 21746921]

4. Wallet P, Lagrange B & Henry T. in Inflammasome Signaling and Bacterial Infections, Current Topics in Microbiology and Immunology. Vol. 397 (ed. Backert S.) 229–256 (Springer, 2016). [PubMed: 27460813]

5. Theisen E & Sauer J-D Listeria monocytogenes and the Inflammasome: From Cytosolic Bacteriolysis to Tumor Immunotherapy. Curr. Top. Microbiol. Immunol. 397, 133–160 (2016). [PubMed: 27460808]

6. Hagar JA, Powell DA, Aachoui Y, Ernst RK & Miao EA Cytoplasmic LPS activates caspase-11: implications in TLR4-independent endotoxic shock. Science 341, 1250–1253 (2013). [PubMed: 24031018]

7. Henry T et al. Type I IFN signaling constrains IL-17A/F secretion by gammadelta T cells during bacterial infections. J. Immunol. 184, 3755–3767 (2010). [PubMed: 20176744]

8. Auerbuch V, Brockstedt DG, Meyer-Morse N, O'Riordan M & Portnoy DA Mice lacking the type I interferon receptor are resistant to Listeria monocytogenes. The Journal of Experimental Medicine 200, 527–533 (2004). [PubMed: 15302899]

9. Woodward JJ, Iavarone AT & Portnoy DA c-di-AMP secreted by intracellular Listeria monocytogenes activates a host type I interferon response. Science 328, 1703–1705 (2010). [PubMed: 20508090]

10. Billiau A & Matthys P Interferon-gamma: a historical perspective. Cytokine Growth Factor Rev. 20, 97–113 (2009). [PubMed: 19268625]

11. Rayamajhi M, Humann J, Penheiter K, Andreasen K & Lenz LL Induction of IFN-alphabeta enables Listeria monocytogenes to suppress macrophage activation by IFN-gamma. The Journal of Experimental Medicine 207, 327–337 (2010). [PubMed: 20123961]

12. Wang Y et al. Inflammasome Activation Triggers Caspase-1-Mediated Cleavage of cGAS to Regulate Responses to DNA Virus Infection. Immunity 46, 393–404 (2017). [PubMed: 28314590]

13. Thackray LB et al. Interferon regulatory factor 5-dependent immune responses in the draining lymph node protect against West Nile virus infection. J. Virol. 88, 11007–11021 (2014). [PubMed: 25031348]

14. Proenca-Modena JL et al. Interferon-Regulatory Factor 5-Dependent Signaling Restricts Orthobunyavirus Dissemination to the Central Nervous System. J. Virol. 90, 189–205 (2016). [PubMed: 26468541]

15. Milligan GN et al. A lethal model of disseminated dengue virus type 1 infection in AG129 mice. J. Gen. Virol. 98, 2507–2519 (2017). [PubMed: 28949904]

16. Rossi SL et al. Characterization of a Novel Murine Model to Study Zika Virus. Am. J. Trop. Med. Hyg. 94, 1362–1369 (2016). [PubMed: 27022155]

17. Müller U et al. Functional role of type I and type II interferons in antiviral defense. Science 264, 1918–1921 (1994). [PubMed: 8009221]

18. McNab F, Mayer-Barber K, Sher A, Wack A & O'Garra A Type I interferons in infectious disease. Nat. Rev. Immunol. 15, 87–103 (2015). [PubMed: 25614319]

19. Stetson DB & Medzhitov R Type I interferons in host defense. Immunity 25, 373–381 (2006). [PubMed: 16979569]

20. Schoenborn JR & Wilson CB Regulation of interferon-gamma during innate and adaptive immune responses. Adv. Immunol. 96, 41–101 (2007). [PubMed: 17981204]

21. Hornung V et al. AIM2 recognizes cytosolic dsDNA and forms a caspase-1-activating inflammasome with ASC. Nature 458, 514–518 (2009). [PubMed: 19158675]

22. Banerjee I et al. Gasdermin D Restrains Type I Interferon Response to Cytosolic DNA by Disrupting Ionic Homeostasis. Immunity 49, 413–426.e5 (2018). [PubMed: 30170814]

23. Liu BC et al. Constitutive Interferon Maintains GBP Expression Required for Release of Bacterial Components Upstream of Pyroptosis and Anti-DNA Responses. Cell Rep 24, 155–168.e5 (2018). [PubMed: 29972777]

24. Kayagaki N et al. Caspase-11 cleaves gasdermin D for non-canonical inflammasome signalling. Nature 526, 666–671 (2015). [PubMed: 26375259]

25. Shi J et al. Cleavage of GSDMD by inflammatory caspases determines pyroptotic cell death. Nature 526, 660–665 (2015). [PubMed: 26375003]

26. Strowig T, Henao-Mejia J, Elinav E & Flavell R Inflammasomes in health and disease. Nature 481, 278–286 (2012). [PubMed: 22258606]

27. Storek KM, Gertsvolf NA, Ohlson MB & Monack DM cGAS and Ifi204 cooperate to produce type I IFNs in response to Francisella infection. J. Immunol. 194, 3236–3245 (2015). [PubMed: 25710914]

28. Paddock CD et al. Rickettsia parkeri rickettsiosis and its clinical distinction from Rocky Mountain spotted fever. Clin. Infect. Dis. 47, 1188–1196 (2008). [PubMed: 18808353]

29. Shi J et al. Inflammatory caspases are innate immune receptors for intracellular LPS. Nature 514, 187–192 (2014). [PubMed: 25119034]

30. Turco J, Liu H, Gottlieb SF & Winkler HH Nitric oxide-mediated inhibition of the ability of Rickettsia prowazekii to infect mouse fibroblasts and mouse macrophagelike cells. Infect. Immun. 66, 558–566 (1998). [PubMed: 9453609]

31. Feng HM & Walker DH Mechanisms of intracellular killing of Rickettsia conorii in infected human endothelial cells, hepatocytes, and macrophages. Infect. Immun. 68, 6729–6736 (2000). [PubMed: 11083788]

32. Turco J & Winkler HH Role of the nitric oxide synthase pathway in inhibition of growth of interferon-sensitive and interferon-resistant Rickettsia prowazekii strains in L929 cells treated with tumor necrosis factor alpha and gamma interferon. Infect. Immun. 61, 4317–4325 (1993). [PubMed: 7691748]

33. Walker DH, Popov VL, Crocquet-Valdes PA, Welsh CJ & Feng HM Cytokine-induced, nitric oxide-dependent, intracellular antirickettsial activity of mouse endothelial cells. Lab. Invest. 76, 129–138 (1997). [PubMed: 9010456]

34. Yamamoto M et al. A cluster of interferon-γ-inducible p65 GTPases plays a critical role in host defense against Toxoplasma gondii. Immunity 37, 302–313 (2012). [PubMed: 22795875]

35. Maltez VI et al. Inflammasomes Coordinate Pyroptosis and Natural Killer Cell Cytotoxicity to Clear Infection by a Ubiquitous Environmental Bacterium. Immunity 43, 987–997 (2015). [PubMed: 26572063]

36. Robinson N et al. Type I interferon induces necroptosis in macrophages during infection with Salmonella enterica serovar Typhimurium. Nat. Immunol. 13, 954–962 (2012). [PubMed: 22922364]

37. Stanley SA, Johndrow JE, Manzanillo P & Cox JS The Type I IFN response to infection with Mycobacterium tuberculosis requires ESX-1-mediated secretion and contributes to pathogenesis. J. Immunol. 178, 3143–3152 (2007). [PubMed: 17312162]

38. Hedges JF et al. Type I Interferon Counters or Promotes Coxiella burnetii Replication Dependent on Tissue. Infect. Immun. 84, 1815–1825 (2016). [PubMed: 27068091]

39. Qiu H et al. Type I IFNs enhance susceptibility to Chlamydia muridarum lung infection by enhancing apoptosis of local macrophages. J. Immunol. 181, 2092–2102 (2008). [PubMed: 18641348]

40. de Almeida LA et al. MyD88 and STING signaling pathways are required for IRF3-mediated IFN-β induction in response to Brucella abortus infection. PLoS ONE 6, e23135 (2011).

41. Engström P et al. Evasion of autophagy mediated by Rickettsia surface protein OmpB is critical for virulence. Nat Microbiol 4, 2538–2551 (2019). [PubMed: 31611642]

42. Man SM et al. The transcription factor IRF1 and guanylate-binding proteins target activation of the AIM2 inflammasome by Francisella infection. Nat. Immunol. 16, 467–475 (2015). [PubMed: 25774715]

43. Aachoui Y et al. Caspase-11 protects against bacteria that escape the vacuole. Science 339, 975–978 (2013). [PubMed: 23348507]

44. Mariathasan S, Weiss DS, Dixit VM & Monack DM Innate immunity against Francisella tularensis is dependent on the ASC/caspase-1 axis. The Journal of Experimental Medicine 202, 1043–1049 (2005). [PubMed: 16230474]

45. Boxx GM & Cheng G The Roles of Type I Interferon in Bacterial Infection. Cell Host Microbe 19, 760–769 (2016). [PubMed: 27281568]

46. Darby AC, Cho N-H, Fuxelius H-H, Westberg J & Andersson SGE Intracellular pathogens go extreme: genome evolution in the Rickettsiales. Trends Genet. 23, 511–520 (2007). [PubMed: 17822801]

47. MacMicking JD Interferon-inducible effector mechanisms in cell-autonomous immunity. Nat. Rev. Immunol. 12, 367–382 (2012). [PubMed: 22531325]

48. Fritsch SD & Weichhart T Effects of Interferons and Viruses on Metabolism. Front Immunol 7, 630 (2016). [PubMed: 28066439]

49. Schindelin J et al. Fiji: an open-source platform for biological-image analysis. Nat. Methods 9, 676–682 (2012). [PubMed: 22743772]

50. Edelstein AD et al. Advanced methods of microscope control using μManager software. J Biol Methods 1, 10 (2014).

51. Jiang Z et al. CD14 is required for MyD88-independent LPS signaling. Nat. Immunol. 6, 565–570 (2005). [PubMed: 15895089]

52. Rauch I et al. NAIP-NLRC4 Inflammasomes Coordinate Intestinal Epithelial Cell Expulsion with Eicosanoid and IL-18 Release via Activation of Caspase-1 and −8. Immunity 46, 649–659 (2017). [PubMed: 28410991]

53. Sauer J-D et al. The N-ethyl-N-nitrosourea-induced Goldenticket mouse mutant reveals an essential function of Sting in the in vivo interferon response to Listeria monocytogenes and cyclic dinucleotides. Infect. Immun. 79, 688–694 (2011). [PubMed: 21098106]

54. Marcus A et al. Tumor-Derived cGAMP Triggers a STING-Mediated Interferon Response in Non-tumor Cells to Activate the NK Cell Response. Immunity 49, 754–763.e4 (2018). [PubMed: 30332631]

55. Purtha WE, Swiecki M, Colonna M, Diamond MS & Bhattacharya D Spontaneous mutation of the Dock2 gene in Irf5−/− mice complicates interpretation of type I interferon production and antibody responses. Proc. Natl. Acad. Sci. U.S.A. 109, E898–904 (2012). [PubMed: 22431588]

56. Szretter KJ et al. 2'-O methylation of the viral mRNA cap by West Nile virus evades ifit1-dependent and -independent mechanisms of host restriction in vivo. PLoS Pathog. 8, e1002698 (2012). [PubMed: 22589727]

57. Fensterl V et al. Interferon-induced Ifit2/ISG54 protects mice from lethal VSV neuropathogenesis. PLoS Pathog. 8, e1002712 (2012). [PubMed: 22615570]

58. Ishida T et al. Endothelial lipase is a major determinant of HDL level. J. Clin. Invest. 111, 347–355 (2003). [PubMed: 12569160]

59. Wang S et al. Murine caspase-11, an ICE-interacting protease, is essential for the activation of ICE. Cell 92, 501–509 (1998). [PubMed: 9491891]

60. Matsuyama T et al. Targeted disruption of IRF-1 or IRF-2 results in abnormal type I IFN gene induction and aberrant lymphocyte development. Cell 75, 83–97 (1993). [PubMed: 8402903]

61. Huang S et al. Immune response in mice that lack the interferon-gamma receptor. Science 259, 1742–1745 (1993). [PubMed: 8456301]
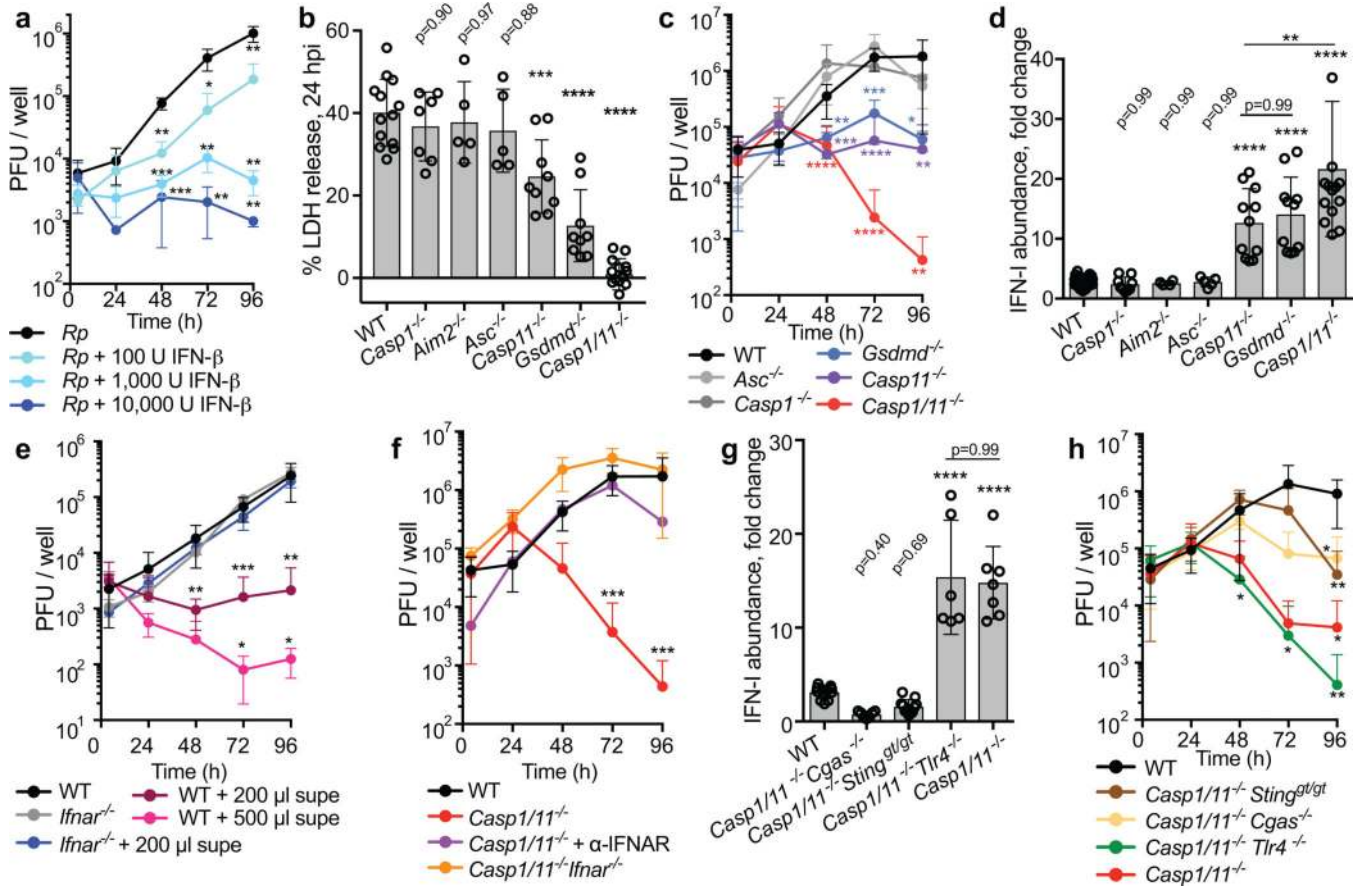
Fig. 1: Inflammasome activation benefits *R. parkeri* by antagonizing the IFN-I response in mouse macrophages

a) *Rickettsia parkeri* (*Rp*) abundance in mouse BMDMs, multiplicity of infection (MOI) 0.2. Recombinant units (U) IFN-β added at 0 hpi. n=3 independent experiments. **b**) BMDM cell death at 24 hpi, as measured by lactate dehydrogenase (LDH) release assay, MOI of 1. From left to right, n=11, 7, 5, 5, 9, 9, and 14 biological replicates. **c**) *R. parkeri* abundance in BMDMs, MOI of 1. n=3 independent experiments. **d**) IFN-I abundance in supernatants of infected BMDMs, MOI of 1, at 24 hpi, using luciferase reporter assay. Data are fold change over uninfected. From left to right, n=30, 9, 4, 5, 11, 11, and 15 biological replicates. **e**) *R. parkeri* abundance in BMDMs, MOI of 0.2. "Supe" indicates conditioned supernatant from infected *Casp1/11*$^{-/-}$ BMDMs. n=3 independent experiments. **f**) *R. parkeri* abundance in BMDMs, MOI of 1. α-IFNAR antibody was added at t=0. n=3 independent experiments. **g**) IFN-I abundance in supernatants of infected BMDMs, MOI of 1, at 24 hpi, using luciferase reporter assay. Data are fold change over uninfected. From left to right, n=11, 7, 11, 6, and 7. **h**) *R. parkeri* abundance in BMDMs, MOI of 1. n=5 independent experiments. In all panels: data are expressed as means ± SD. *p<0.05, **p<0.01, ***p<0.001, ****p<0.0001, ns=not significant; statistical analyses in panels a, c, e, f, and h were performed using a two-tailed Student's T-test, compared to WT or the control; statistical analyses in panels b, d, and g were performed using a one-way ANOVA with multiple comparisons and Tukey post-hoc test.
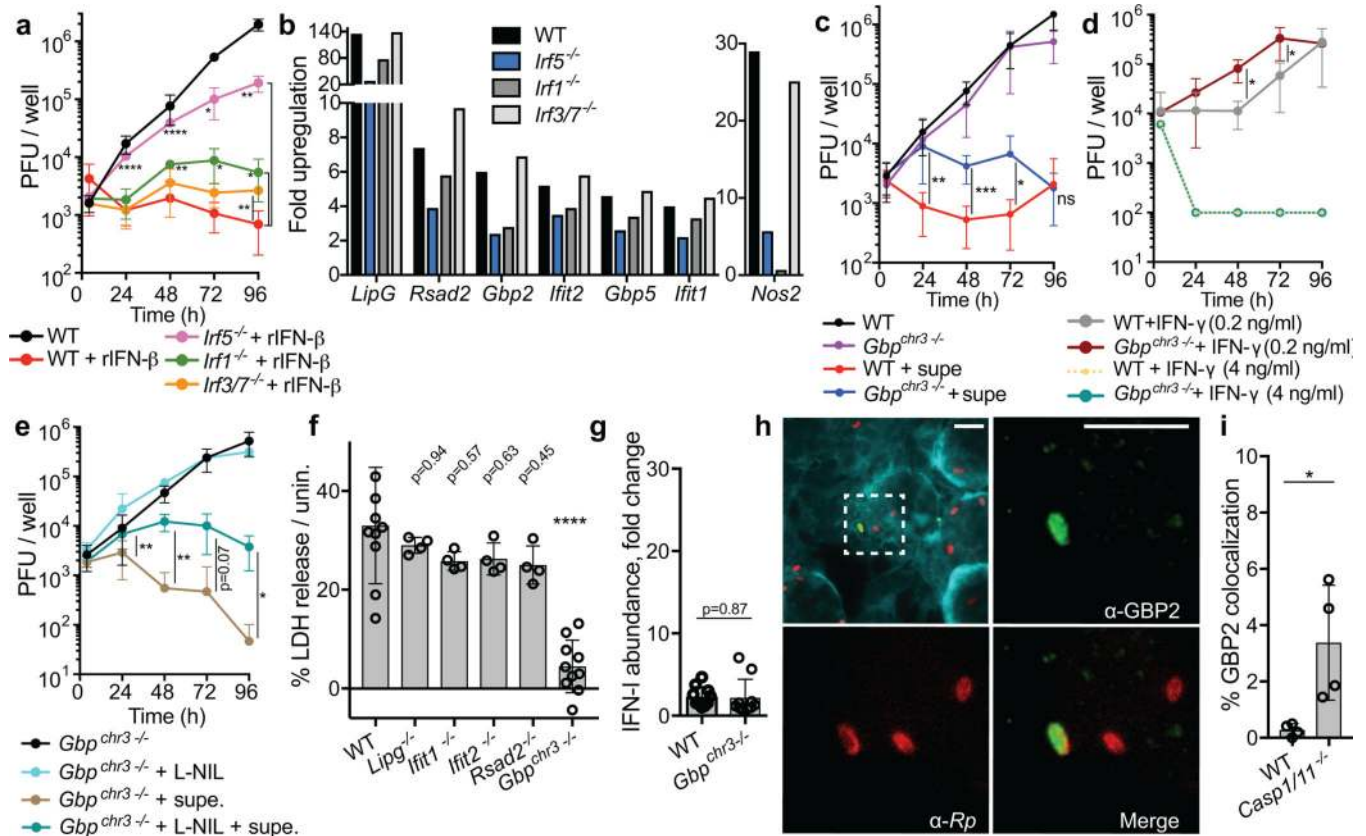
Fig. 2: Inflammasome activation enables *R. parkeri* to avoid stimulating anti-rickettsial ISGs

a) *R. parkeri* abundance in BMDMs, MOI of 0.2. 10,000 units of recombinant IFN-β (rIFN-β) added at 0 hpi. n=3 independent experiments. Statistical comparisons were made between infected mutant cells and infected WT BMDMs treated with IFN-I. **b**) Transcript abundance by RNAseq of IFN-I-stimulated IRF5-regulated genes, from highest to lowest by upregulation in WT cells. *Nos2* shown separately, as it was more highly regulated by IRF1. Data are from one experiment. **c**) *R. parkeri* abundance in BMDMs, MOI of 0.2. "Supe" indicates 500 μl of supernatant collected at 24 hpi from infected *Casp1/11⁻/⁻* BMDMs. n=3 independent experiments. **d**) *R. parkeri* abundance in BMDMs, MOI of 1. IFN-γ was added at t=0. n=3 independent experiments. **e**) *R. parkeri* abundance in BMDMs, MOI of 0.2. "Supe" is 500 μl supernatant from infected *Casp1/11⁻/⁻* cells, added at 0 hpi. The L-NIL final concentration was 1 mM, added at t=0. n=3 independent experiments **f**) BMDM cell death at 24 hpi, as measured by LDH release assay, MOI of 1. From left to right, n=10, 4, 4, 4, 4, and 10 biological replicates. Statistical comparisons were made to WT. **g**) IFN-I abundance in supernatants of infected BMDMs, MOI of 1, at 24 hpi, using luciferase reporter assay. Data are fold change over uninfected. n=10 and 10 biological replicates. **h**) Representative image using 100x confocal immunofluorescence microscopy of WT BMDMs treated with 100 U rIFN-β overnight, infected with *R. parkeri,* 3 hpi, MOI of 1. Cyan staining is phalloidin; green staining is α-GBP2; red staining is α-*Rickettsia.* Scale bars = 5.6 μm. Data represent 4 independent experiments. **i**) Quantification of GBP2 and *R. parkeri* co-localization at 24 hpi. Each data point is an average of at least 5 separate images totaling >150 bacteria, each from an independent experiment, n=4. For all panels, data are expressed

as means and error bars represent the SD; *p<0.05, **p<0.01, ***p<0.001, ****p<0.0001, ns=not significant; statistical analyses in panels a, c, d, e, g, and i used a two-tailed Student's T-test; statistical analyses in panel f used a one-way ANOVA with multiple comparisons and Tukey post-hoc test.
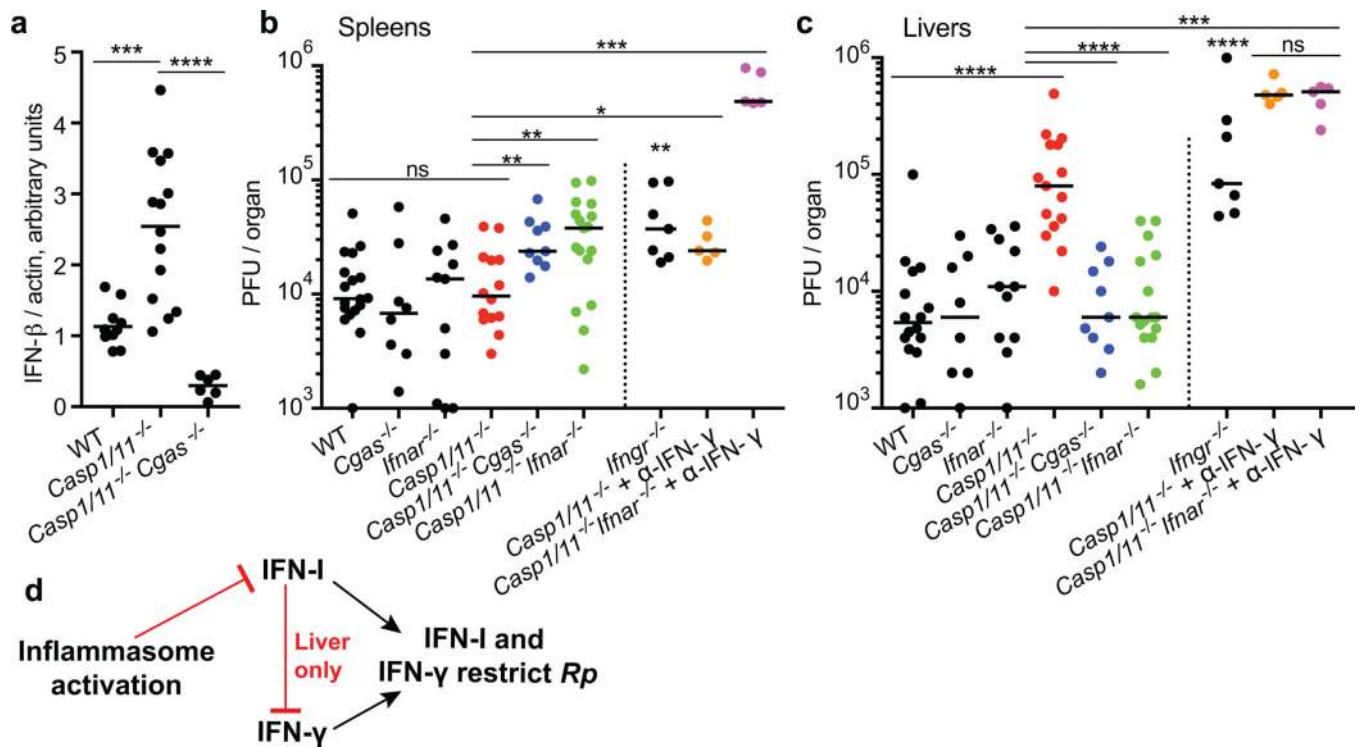
Fig. 3: Inflammasome activation *in vivo* antagonizes IFN-I production, benefitting *R. parkeri* in the spleen and benefiting the host in the liver

a) IFN-β transcripts quantified using qPCR, at 72 hpi in spleens of C57BL/6 mice, infected i.v. with 10^7 PFU. From left to right, n=11, 14, and 6 individual mice. **b**) *R. parkeri* abundance in mouse spleens, infected i.v. with 10^7 PFU, at 72 hpi. Bars denote medians. From left to right, n=18, 8, 11, 14, 9, 17, 7, 5, and 5 individual mice. **c**) *R. parkeri* burdens in livers, i.v. at 72 hpi. From left to right, n=16, 8, 11, 15, 9, 16, 7, 5, and 5 individual mice. Horizontal lines represent medians; data to the right of the dotted lines pertain to IFN-γ and are separated for clarity. Data for each group are combined from ≥3 independent experiments, with the exception of neutralization experiments, which are 2 independent experiments; statistical analyses for *Ifngr*$^{-/-}$ are compared to WT; statistical analyses in panel a used a one-way ANOVA with multiple comparisons and Tukey post-hoc test; statistical analyses in panels b and c used a two-tailed Mann Whitney *U* test; *p<0.05, **p<0.01, ***p<0.001, ****p<0.0001, ns=not significant. **d**) Textual summary of results from panels a, b, and c. Rp, *Rickettsia parkeri*.
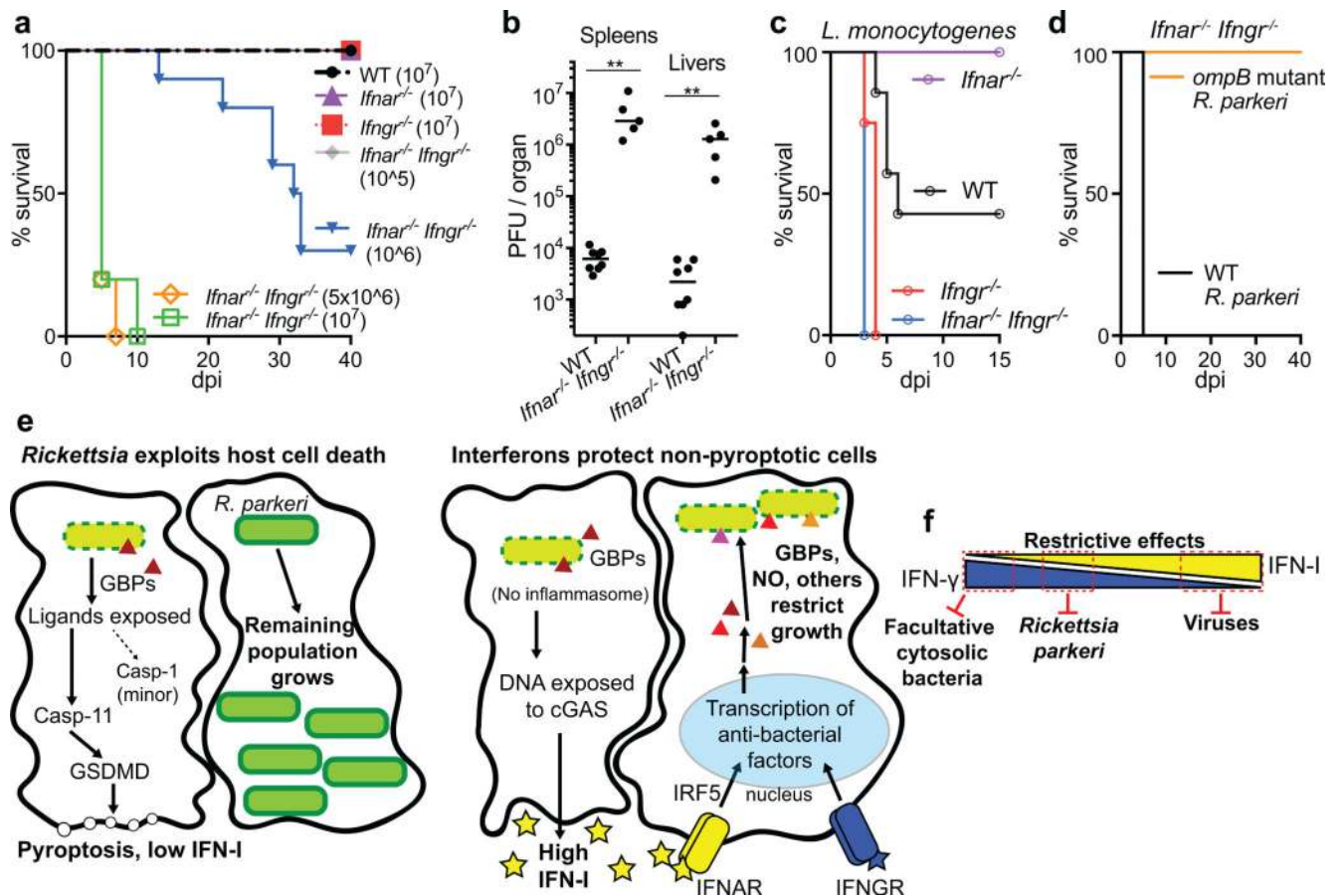
Fig. 4: IFN-I and IFN-γ play critical and overlapping roles in controlling *R. parkeri* in mice
a) Survival of C57BL/6 mice upon i.v. infection with *R. parkeri*. n=5 (WT), 10 (*Ifnar*$^{-/-}$), and 8 (*Ifngr*$^{-/-}$) individual mice; for *Ifnar*$^{-/-}$*Ifngr*$^{-/-}$ n=8 (10^5), 10 (10^6), 5 (5×10^6), and 5 (10^7) individual mice. **b**) *R. parkeri* abundance in mouse organs after i.v. delivery of 10^7 PFU, at 72 hpi. n=8 (WT) and 5 (*Ifnar*$^{-/-}$*Ifngr*$^{-/-}$), individual mice; horizontal bars denote medians; statistical analyses used a two-tailed Mann-Whitney *U* test; **p<0.01. **c**) Mouse survival upon i.v. delivery of 4×10^3 WT *L. monocytogenes*. n=6 (*Ifnar*$^{-/-}$), 7 (WT), 8 (*Ifngr*$^{-/-}$), and 6 (*Ifnar*$^{-/-}$*Ifngr*$^{-/-}$) individual mice. **d**) Survival of *Ifnar*$^{-/-}$*Ifngr*$^{-/-}$ mice upon i.v. delivery of 10^7 WT or *ompB* mutant *R. parkeri*. n=5 (WT) and 7 (*ompB* mutant) individual mice. For all panels, data are the combination of two independent experiments. **e**) Model depicting intracellular growth of *R. parkeri* in WT cells (left) or in cells lacking inflammasome signaling (right). NO, nitric oxide. **f**) Model for the antimicrobial effects of interferons on cytosolic pathogens.